HHS Public Access

Author manuscript

Neuroscience. Author manuscript; available in PMC 2015 March 18.

Published in final edited form as:

Neuroscience. 2013 March 1; 232: 32–44. doi:10.1016/j.neuroscience.2012.11.023.

VMAT1 Deletion Causes Neuronal Loss in the Hippocampus and Neurocognitive Deficits in Spatial Discrimination

Pushpinder K. Multani[1], **Rachel Hodge**[1], **Marcel A. Estévez**[3], **Ted Abel**[1,3], **Hank Kung**[2], **Mark Alter**[1], **Bethany Brookshire**[1], **Irwin Lucki**[1,2], **Aleksandra H. Nall**[1], **Konrad Talbot**[1], **Glenn A. Doyle**[1], and **Falk W. Lohoff**[1,*]

[1]Center for Neurobiology and Behavior, Department of Psychiatry University of Pennsylvania School of Medicine Translational Research Laboratories, Philadelphia, PA

[2]Departments of Pharmacology and Radiology, University of Pennsylvania School of Medicine, Philadelphia, PA

[3]Department of Biology, University of Pennsylvania, Philadelphia, PA

Abstract

Vesicular monoamine transporters (VMAT) are involved in presynaptic storage and release of neurotransmitters. While it was thought initially that only VMAT2 is brain expressed and VMAT1 is present only in the periphery, recent data has challenged the exclusive expression of VMAT2 in brain. To further elucidate the role of VMAT1 brain expression and its potential role in neuropsychiatric disorders, we have investigated mice lacking VMAT1. Comparison of wildtype and knock-out (KO) mice using qPCR and immunohistochemistry documents the expression of VMAT1 in the brain. Deletion of VMAT1 leads to increased hippocampal apoptosis and reduced neurogenesis as assessed by caspase-3-labeling and BrdU-labeling. Behavioral data show that mice lacking VMAT1 have neurocognitive deficits. VMAT2 expression is not altered in VMAT1 KO mice, suggesting a distinct role of VMAT1. Our data support VMAT1 brain expression and suggest that VMAT1 plays a key role in survival of hippocampal neurons and thus might contribute to neurocognitive deficits observed in neuropsychiatric disorders.

Keywords

SLC18A1; VMAT2; apoptosis; neurogenesis; cognition; hippocampus; schizophrenia; bipolar disorder

*Corresponding author: Falk W. Lohoff, MD, Assistant Professor of Psychiatry, University of Pennsylvania School of Medicine, Department of Psychiatry, Center for Neurobiology and Behavior, Translational Research Laboratories, 125 South 31st Street, Room 2213, Philadelphia, PA 19104, Office: (215) 573-4582, Fax: (215) 573-2041, lohoff@mail.med.upenn.edu.

Introduction

Vesicular monoamine transporters (VMATs) are located presynaptically and transport monoamines into storage vesicle that release their content upon arrival of an action potential. In human, two structurally related but pharmacologically distinct VMATs exist, encoded by separate genes, *VMAT1* (*SLC18A1*) located on chromosome 8p21 and *VMAT2* (*SLC18A2*) located on chromosome 10q25 (Liu et al., 1992, Peter et al., 1993, Erickson et al., 1996). Although it was thought initially that only VMAT2 is expressed in brain and VMAT1 not (Peter et al., 1995, Erickson et al., 1996), the exclusive brain expression of VMAT2 has been recently challenged by data that show VMAT1 in mouse, rat, and human brain (Hansson et al., 1998, Lohoff et al., 2006, Ibanez-Sandoval et al., 2010, Ashe et al., 2011). VMATs are structurally similar to other plasma membrane transporters, such as the dopamine transporter (DAT), serotonin transporter (SERT), and norepinephrine transporter (NET), with 12 transmembrane domains and both termini located in the interior (Liu et al., 1992). Nevertheless, VMAT physiology differs from plasma membrane transporters in that they use a proton gradient to transport substrates and lack an extracellular compartment. Both VMAT1 and VMAT2 are able to transport monoamines; however, they have distinct substrate preferences and affinities. VMAT1 has higher affinity for serotonin (Brunk et al., 2006), whereas VMAT2 is also able to transport histamine (Erickson et al., 1996).

The importance of VMAT2 in monoamine signaling has been clearly documented using various approaches, including rodent animal models. Studies of mice lacking VMAT2 show that the homozygote animals die within a few days of birth and heterozygotes have significantly decreased monoamine levels and increased neurotoxicity as well as depressive-like phenotypes (Fon et al., 1997, Takahashi et al., 1997, Wang et al., 1997, Fumagalli et al., 1999, Narboux-Neme et al., 2011). Numerous other preclinical studies have shown that drugs of abuse have robust effects on VMAT2 function/expression, including increased neurotoxicity after methamphetamine exposure (Fumagalli et al., 1999, Uhl et al., 2000, Hall et al., 2003, Savelieva et al., 2006, Fleckenstein et al., 2007, Vergo et al., 2007, Yamamoto et al., 2007, Tong et al., 2008, Fleckenstein et al., 2009, Eiden and Weihe, 2011, Ellis et al., 2011, McFadden et al., 2011a, McFadden et al., 2011b, Vieira-Brock et al., 2011). Caudle et al (2007) observed that mice expressing approximately 5% of normal VMAT2 (VMAT2 LO) display age-associated nigrostriatal dopamine dysfunction accompanied by increased oxidative stress and decreased expression of the dopamine transporter and tyrosine hydroxylase, ultimately leading to neurodegeneration (Caudle et al., 2007). Genetic disruption of *VMAT2* also increased apoptotic cell death in cortex (Stankovski et al., 2007).

Given the fundamental importance of VMAT2 in monoamine signaling and neuronal survival, and new evidence of VMAT1 brain expression, VMAT1 represents an interesting new target for investigation. Furthermore, several reports have shown that common missense variants in human *VMAT1* are associated with bipolar disorder (BPD), schizophrenia (SZ), anxiety-related personality traits and cognitive phenotypes related to SZ (Bly, 2005, Lohoff et al., 2006, Richards et al., 2006, Chen et al., 2007, Lohoff et al., 2008a, Lohoff et al., 2008b, Need et al., 2009). This is remarkable since the human *VMAT1* gene is located on chromosome 8p, a region previously implicated as a shared genomic susceptibility region for SZ/BPD in linkage scans. The fact that several common missense

variations in this gene have been associated with different psychiatric phenotypes suggests that certain fundamental neurobiological mechanisms are shared between psychiatric phenotypes, leading to pleiotropy.

In this study we report for the first time cellular, molecular and behavioral consequences in mice lacking VMAT1. Based on human association data of VMAT1 variants with cognitive phenotypes (Need et al., 2009) and substantial evidence of hippocampal dysfunction with psychosis in SZ/BPD and other neuropsychiatric phenotypes (Benes et al., 1998, Tamminga et al., 2010, Konradi et al., 2011) we specifically investigated the effect of *VMAT1* deletion on hippocampal processes. We find that disruption of the *VMAT1* gene enhanced apoptosis in the dentate gyrus that was accompanied by reduced cell proliferation in the hippocampus of *VMAT1*KO mice. Furthermore, the hippocampus-dependent spatial object recognition behavioral task was disrupted in the *VMAT1*KO mouse. The combined effect of apoptosis and reduced neurogenesis coupled with a concomitant cognitive behavioral deficit suggests that these mice may be useful to further study effects of abnormal monoaminergic signaling on hippocampal function.

Material and Methods

Animals

*VMAT1*KO mice (B6.129P2-*Slc18a1*^{tm1Dgen}/J) were created at Deltagen (http://www.deltagen.com/) and obtained from the Jackson Laboratories (strain stock no. 006432). Animals (body weight 22-25g) were housed in groups of 2-4 in polycarbonate cages and maintained on a 12-h light/dark cycle in a temperature (22°C) and humidity controlled room. Animal procedures were conducted in accordance with the guidelines published in the National Institute of Health Guide for Care and Use of Laboratory Animals. All protocols were approved by the University of Pennsylvania's Institutional Animal Care and Use Committee.

Genomic Structure of *VMAT1KO* mice

The genomic structure of the *VMAT1KO* was verified by amplification and sequencing of the junctions between the endogenous mouse DNA and the inserted IRES/LacZ/Neo cassette (Fig. 1A). The 5′ boundary was amplified using a forward primer within exon 4 (5′-GGTACCATCCCTCCTCCAGT-3′) and a reverse primer within the LacZ sequence (5′-TGCTGCAAGGCGATTAAGTTGGGTAACG-3′). The 3′ boundary was amplified using a forward primer within the Neo^{R} region (5′-AGGATCTCCTGTCATCTCACCTTGCTCCTG-3′) and a reverse primer within intron 4 (5′-GTACTAACCTTCTGAAACTGTAAGCAAGCC-3′). PCR amplicons were gel purified using Qiaquick spin columns (Qiagen), and sequenced directly using the amplification primers. Sequence data showed that the IRES/LacZ/Neo cassette replaces 61 basepairs of sequence located 264 basepairs downstream of the start of exon 4 (data not shown).

Genotyping of *VMAT1KO* Mice

To genotype WT, heterozygous and homozygous *VMAT1KO* mice, tail DNA was extracted and purified using Proteinase K digestion followed by either chloroform extraction and

ethanol precipitation or bead-based purification using an iPrep machine (Invitrogen, Carlsbad, CA). Multiplex PCRs were performed with two forward primers, one located in the endogenous intron 3 mouse sequence upstream of the insertion (5′-GCATGGATAAATGGTACCATCCCTC-3′), a second located in the 3′ end of the insertion (5′-GGGTGGGATTAGATAAATGCCTGCTCT-3′), and one reverse primer located in the endogenous intron 4 mouse sequence downstream of the insertion (5′-CACAGCAATAGAGCAGTGACTAAGAC-3′). A 227 base pairs band was expected for WT animals, a 479 base pairs band was expected for homozygous knock out animals, and both bands were expected for heterozygotes (Fig. 1B).

Gene Expression Assays

VMAT1 mRNA expression was assessed in frontal cortex, striatum, hippocampus and adrenal glands dissected and pooled from either five wild type (WT), four heterozygous or three homozygous *VMAT1*KO mice using TaqMan Gene Expression Assays. Three micrograms total RNA, extracted using Trizol Reagent (Invitrogen), was converted to cDNA using the SuperScriptII First-Strand Synthesis Kit (Invitrogen). A custom *VMAT1* TaqMan Gene Expression Assay (Applied Biosystems, ABI), designed to span from within the deletion in exon 4 to exon 5, was used. Inventoried TaqMan Gene Expression Assays (ABI) for *VMAT1* (Mm_01345494_m1), *VMAT2 (*Mm_00553058_m1) and *GapdH*, as a normalizer gene, were also done. Real-time quantitative PCR was performed in a 20 ul reaction containing 10 ul of 2× TaqMan Universal PCR Master Mix (ABI), 1 ul of 20× TaqMan Gene Expression Assay (ABI), and cDNA. Reactions, done in triplicates, were cycled 40 times in an ABI 7900HT under the manufacturer's recommended conditions. Change in cycle threshold (ΔCt) values were calculated by subtracting the *GapdH* Ct value from the various *VMAT* Ct values. Fold change was calculated relative to the WT values for each tissue for each assay using the ΔΔCt method and the equation $2^{-(\Delta\Delta Ct)}$.

Immunohistochemistry

Male WT and *VMAT1*KO animals (8-12 wks, n=5) were anesthetized (Nembutal, 10mg/kg, i.p.) and perfused transcardially with heparinized saline (1000 units/ml) and buffered formalin. Adrenal glands were removed and embedded in paraffin to make 6 μm slices. Brains were post-fixed in buffered formalin in the skull for 24 h, then outside the cranial cavity for an additional 24 h, cryoprotected in 30% sucrose, and frozen in liquid isopentane at −40°C. Forty micron-thick coronal sections were cut to form frozen brain slice slides for VMAT1 and VMAT2 immunostaining as well as free floating brain slices for caspase-3 staining. For VMAT1 and VMAT2, an antigen retrieval step was done by incubating brain or adrenal slices in heated (85°C) citrate-based antigen retrieval solution (Vector Laboratories, CA) for 20 min. The prefrontal cortex, striatum, hippocampus and adrenal gland were blocked for 1h at room temperature with Tris-buffered Saline (TBS) containing 5% normal horse serum, 0.5% Tween 20 and 0.1% Triton (blocking solution). Sections were then incubated overnight at 4°C in 1:2500 rabbit anti-caspase-3, (Cell signaling, #9662), 1:1000 rabbit anti-VMAT1 (Santa Cruz, SC15313) or 1:1000 rabbit anti-VMAT2 (Abcam, ab87594) primary antibody diluted in blocking solution. Sections were washed and incubated for 2 h in donkey anti-rabbit secondary antibody (Vector Laboratories) diluted 1:500 in blocking solution. Sections were then washed and treated with 1:3:6

H_2O_2:Methanol:TBS for 15 min at room temperature before incubation in avidin-biotin (Vector Laboratories, PK6100) diluted 1:6 in TBS containing 0.5% BSA. For VMAT1 or VMAT2, labeled cells were visualized using Nickel-diaminobenzidine (Vector Laboratories, DAB kit SK4100) whereas caspase-3 staining was visualized with diaminobenzidine only followed by counterstaining with hematoxylin. As negative control, one to two sections from each animal were incubated with all reagents except the primary antibodies. Free-floating sections were mounted onto slides and dried for 72 h before dehydrating and cover slipping with Permount. Images were captured on an Olympus microscope equipped with DP70 digital camera and DP Olympus software. Quantification of the cell counts was done as described (Soetanto et al., 2010).

Double Immunolabeling for VMAT1 and Synaptophysin

Male WT (8-12 wks, n=4) were anesthetized (Nembutal, 10mg/kg, i.p.) and perfused transcardially with heparinized saline (1000 units/ml) and buffered formalin. Brains were removed and embedded in paraffin to make 6 μm slices. For VMAT1 an antigen retrieval step was done by incubating brain slices in heated (85°C) citrate-based antigen retrieval solution (Vector Laboratories, CA) for 20 min. The prefrontal cortex, striatum and hippocampus were blocked for 1h at room temperature with Tris-buffered Saline (TBS) containing 5% normal horse serum, 0.5% Tween 20 and 0.1% Triton (blocking solution). Sections were then incubated in a primary antibody mixture (1:1000 rabbit anti-VMAT1 Santa Cruz, SC15313, 1:1000 mouse anti-synaptophysin clone Sy38, Dako company) diluted in blocking solution at 4°C overnight. Sections were washed and incubated for 2 h in a mixture of Alexa 488 anti-rabbit (1:500) and Alexa 594 anti- goat (1:500) secondary antibody (Jackson immuno research labs) diluted 1:500 in blocking solution. Images were captured on an Olympus fluorescent microscope equipped with DP70 digital camera and DP Olympus software.

Quantitative immunohistochemistry (qIHC)

A protocol by (Soetanto et al., 2010) was employed in which all sections to be compared for a given antigen were reacted simultaneously with the same solutions for the same amount of time using a standard procedure as described above. On each cover slipped slide, we outlined in ink the region of interest (ROI), Using the same lighting conditions for all sections in a given IHC experiment, gray-scale photomicrographs at 100× covering the ROI were taken on a Leitz DMRB microscope (Leica Microsystems, Wetzlar, Germany) equipped with a Retiga Exi/QEi digital camera (QImaging, Surrey, BC, Canada) distinguishing 4095 shades of gray and with a MAC 2000 motorized stage (Ludl Electronic Products, Hawthorne, NY) driven by the Turboscan feature of Image-Pro Plus software (Media Cybernetics Inc., Silver Springs, MD, USA). That software was used to create composite images of the entire ROI in each section and to quantify relevant features of the images: (a) neuronal parameters (areas of cell nuclei and cell bodies), (b) immunoreactive neurons per mm^2 where “neuron” was defined as an immunoreactive cell larger than the maximal size of cell nuclei (70.4 μm^2) as measured in hematoxylin-stained sections from our tissue samples.

Western Blotting

Animals were decapitated under Nembutal (10 mg/kg, i.p.) anesthesia. The hippocampus was dissected and both hemispheres combined before being placed in 1X radio-immunoprecipitation assay (RIPA) buffer containing the following enzyme inhibitors: 1 tablet/10ml Complete Mini (Roche), 20 μg/ml Pepstatin A (Sigma) and 50 mM Sodium Vanadate (Fisher). Tissue samples were sonicated, centrifuged at 14,000*g* for 10 min, and the supernatant was used for all immunoblot analysis. Samples (50 μg total protein/well) were separated by electrophoresis on 4-12% Tris-bis gels using MES buffer (Invitrogen), transferred to nitrocellulose (Invitrogen) and membranes blocked with 5% dry milk in TBS containing 0.1% Tween-20 (TBST) for 60 min at room temperature. Caspase-3 activation was detected using a 1:1000 dilution of a rabbit anti-caspase-3 antibody (Cell signaling, #9662) in TBST blocking solution with 0.5% BSA overnight at 4°C. Membranes were washed, incubated with a 1:10,000 dilution of horseradish peroxidase (HRP)-conjugated secondary antibody (Jackson labs) for 1 h at room temperature and developed using enhanced chemiluminescence (ECL) kit (GE Healthcare). As a loading control, membranes were then re-probed with a 1:1000 dilution of mouse anti-β-actin antibody (Millipore; clone C-4, MAB1501). Blots were again washed and β-actin detected using ECL after incubation with a 1:10,000 dilution of HRP-conjugated anti-mouse IgG secondary antibody (Jackson Labs). Protein expression was quantified by densitometry with Image J software (http://rsb.info.nih.gov/ij/index.html). The pro and active caspase-3 bands were normalized to the β-actin band.

Electron Microscopy

Hippocampal tissue used in brain slice preparations was obtained from 8-12 week old male WT and *VMAT1*KO mice. Brain slices for electron microscopy were prepared following the protocol described by (Larimore, 2011). Electron microscopy was performed with a JEOL 1010 electron microscope fitted with a Hamamatsu digital camera. Images were acquired with AMT advantage image capture digital software (Version 542).

Hippocampal Cell Proliferation

The effect of VMAT1 deletion on cell proliferation was determined by measuring the incorporation of 5-bromo-deoxy-uridine (BrdU) into the hippocampus. Mice were injected intraperitoneally with 200mg/kg BrdU (Roche Applied Sciences; Indianapolis, IN) in a volume of 10ml/kg 24 hours prior to sacrifice. To analyze cell proliferation, male mice (WT, n=10; *VMAT1*KO, n=10) were sacrificed 24 h after the last BrdU injection and incorporation of BrdU into the hippocampus was measured using flow cytometry as described (Balu et al., 2009). Data were collected on a BD FACS Canto System (BD Biosciences) at the University of Pennsylvania's Flow Cytometry Core Facility. Data collected from a BrdU-free sample controlled for background signals. All data were analyzed using BD FACS Diva Software (BD Biosciences).

Spatial Object Recognition Task

The experimental apparatus was a rectangular open field (50×33×40 cm) with a visual cue placed on the arena wall. Prior to training, mice were handled for 2 min a day for 3 days.

During the training day, male mice received four 10-min training sessions. Between sessions, mice were put back in their home cage for 3 min. During the first session, mice were habituated to the rectangular open field in the absence of objects, but with an internal visual cue on one of the four walls. During the next three sessions, mice were placed in the same box but now with two distinct objects such as a glass bottle with white opaque filling and an empty glass flask. Mice were allowed to freely explore the environment and the objects for 10 min. After 24 h, mice were placed back in the rectangular environment for the testing phase. The two objects were again present, but one of the two objects was now displaced to a novel spatial location with respect to the internal visual cue. Mice were again allowed to freely explore the environment and the objects for 6 min. Time spent exploring the displaced and non-displaced objects was measured. The identity of the objects as well as the spatial location in which the objects were located was balanced between subjects.

Contextual Fear Conditioning

Male mice (WT, n= 8; *VMAT1KO*, n= 8) were handled for three consecutive days for 1 min each day prior to conditioning. On the training day, mice were placed into the conditioning chamber (MED Associates, East Fairfield, VT) and received a 2-sec (1.5-mA) scrambled footshock 2.5 min after placement into the chamber. Mice were removed from the chamber after 3 min. During testing, mice were exposed to the same context for 5 min, without the presentation of footshock. Freezing was scored using FreezeScan (CleverSys, Inc.) at 1-min intervals and the percentage of those intervals in which the mouse froze was calculated.

Biodistribution study

The distribution of VMAT2 was measured in WT, VMAT1KO, and VMAT2 heterozygote mice (24-33g, 8-12 weeks old, n=4 per group) using [^{18}F]-AV-133 as ligand. Each animal was injected with 0.15ml of a saline solution containing 20uCi of [^{18}F] AV-133 was injected directly into the tail vein of mice under isoflurane anesthesia. The mice were sacrificed by cardiac excision at 60 minutes after injection. Various organs such as kidney, liver, pancreas, bone and brain were removed and weighed, and the radioactivity was counted with an automatic gamma counter (1480 Wizard 3″, Perkin-Elmer). The percentage dose per gram of tissue was calculated by a comparison of the tissue counts to diluted aliquots of the injected material.

Ex vivo autoradiography of [18F] AV-133

1.6mCi of [^{18}F]AV-133 was injected into the tail vein of mice under isofluorane anesthesia. The mice were sacrificed at 60 min after [^{18}F]AV-133 injection. The brains were removed and frozen with powdered dry ice. Frozen brains were sectioned (25um) in the coronal plane and air-dried in front of a fan. Sections were exposed to Biomax MR films for overnight and films were processed with Kodak fixer and developer. Images were digitized with an Epson Perfection 4490 Photo scanner.

Data Analysis

Two-tailed non-parametric Student's t-test was employed for the statistical analysis of between-group differences (WT *versus* *VMAT1*KO). *P* values < 0.05 were considered to be statistically significant.

Results

Characterization of *VMAT1*KO Mice and Expression of VMAT1 in Brain

Various approaches were used to assess whether VMAT1 mRNA and protein expression were absent in various brain regions and adrenal gland of *VMAT1*KO mice. We first confirmed that the gene trap cassette insertion caused a 61 bp deletion located within exon 4 of the *VMAT1* gene (Fig. 1A). Further characterization of WT, heterozygous and homozygous *VMAT1*KO mice (representative genotypes shown in Fig. 1B) by quantitative RT-PCR of various brain regions and adrenal gland, chosen because VMAT1 is highly expressed in adrenal medulla (Peter et al., 1995), confirmed the presence of *VMAT1* mRNA in WT and heterozygous mice as well as its absence in homozygous *VMAT1*KO mice (Fig. 1C).

To obtain an overview of VMAT1 expression in the adult mouse brain, frozen sections from different regions were analyzed for VMAT1-immunoreactivity (ir) using a specific anti-VMAT1 antibody (SC15313). High power images of immunohistochemical analyses of different regions of adult WT mouse brain revealed intracellular distribution of VMAT1-ir that was broadly expressed within several areas, especially the prefrontal cortex, striatum and dentate gyrus (Fig. 2A, panels D, F, H). In the hippocampus, VMAT1-ir was present in all regions, with the highest density of positive cells in the molecular and granule cell layers (Fig. 2 panel H). As expected, adrenal gland also showed strong VMAT1-ir (Fig. 2J, L). Importantly, immunohistochemical staining of various brain regions and adrenal gland from *VMAT1*KO mice with either SC15313 or a custom designed VMAT1-specific antibody (data not shown) showed no VMAT1-ir. Double-immunofluorescence of VMAT1 with synaptophysin (Fig.2B), a presynaptic vesicle protein marker, shows VMAT1 is located in synapses. Taken together, these data (Fig. 2A,B), combined with the *VMAT1* RT-PCR data (Fig. 1C), confirmed the presence of VMAT1 expression in WT mouse brain and adrenal gland as well as its absence in the *VMAT1*KO mice.

Absence of VMAT1 Increases Apoptotic Cell Death in the Dentate Gyrus

Genetic disruption of *VMAT2* increases apoptotic cell death in cortex (Stankovski et al., 2007). Thus, various experimental techniques were employed to determine whether lack of *VMAT1* expression also induces cell death by apoptosis. Immunohistochemical staining of caspase-3, activation of which is a hallmark of apoptosis, was quantified in cortex, striatum and hippocampus from WT and *VMAT1*KO mice (Fig. 3). Whereas the granule cell layer of dentate gyrus of *VMAT1*KO mice showed a 140% increase ($p<0.001$) in caspase-3 positive cells compared to WT littermates (Fig. 3A, B), neither the cortex nor striatum showed differential caspase-3 labeling between WT and *VMAT1*KO mice (Fig. 3B). Light microscopy revealed a neuronal morphology of cells stained positive for caspase-3, with cytosolic staining being present in the soma as well as in dendrites. During caspase-3

zymogen activation, the 32 kDa pro-enzyme form is cleaved to an active 17 kDa fragment by caspase-dependent processes. Thus, although our immunohistochemical data suggested increased apoptosis in the dentate gyrus as an effect of VMAT1 deficiency, we analyzed the cleavage state of caspase-3 in hippocampi from WT and *VMAT1*KO mice by Western immunoblot (Fig. 3C). The level of the 17 kDa cleavage product of caspase-3 was significantly higher ($p<0.01$) in the hippocampus of *VMAT1*KO as compared to WT mice (Figs. 3D). Therefore, the increase in cleaved, active caspase-3 protein levels in *VMAT1*KO mice suggests enhanced neuronal cell death in the hippocampus by apoptosis.

Electron microscopic evaluation of hippocampal neurons revealed that the cellular profiles in *VMAT1*KO mice also displayed the classical features of apoptosis. Whereas WT neurons showed normal nuclear morphology (Fig. 4A), *VMAT1*KO neurons showed fragmented nuclear membranes with nuclear chromatin condensation into one or more large geometrically spherical dense balls. Furthermore, cells were condensed and subdivided into numerous small bodies, each containing one or more spherical clumps of nuclear chromatin surrounded by a contingent of cytoplasm (Figs. 4B-D).

Hippocampal Cell Proliferation is Decreased in *VMAT1*KO Mice

To determine the effects of VMAT1 deletion on cell proliferation, the incorporation of BrdU into the hippocampus of WT and *VMAT1*KO mice was assessed by the method of Balu et al (2009). *VMAT1*KO mice had a significantly ($t(16)=2.78$, $p=0.01$) lower (70%) level of hippocampal cell proliferation as compared to WT mice (Fig. 5).

Spatial Object Recognition, but not Contextual Fear Conditioning, is Disrupted in *VMAT1*KO Mice

We next assessed *VMAT1*KO and WT mice for performance in learning paradigms that depend on normal hippocampal function. Whereas spatial memory formation was affected in *VMAT1*KO mice using the spatial object recognition (SOR) task (Fig. 6A, B), no effect on contextual fear conditioning (CFC) was observed (Fig. 6C). In the SOR task, WT mice preferentially explored the displaced object, whereas, in contrast, *VMAT1*KO mice failed to discriminate between the displaced and non-displaced objects (Fig. 6A; 65.0±0.76%, WT; 52.5±0.81%, *VMAT1*KO; $p<0.01$). Importantly, total exploration time was not different between the two groups (Fig. 6B). Lastly, another cohort of WT and *VMAT1*KO mice were studied for CFC. In CFC, mice learn to associate a specific environmental context with a foot shock. This task requires the function of the hippocampus and amygdala. When *VMAT1*KO mice and WT littermates were re-exposed to the same context 24 h after training, they showed no significantly different levels of freezing (Fig. 6C; 64.4±4.2%, WT; 59.0±5.0%, *VMAT1*KO; $p=0.40$). Taken together, these data indicate that VMAT1 is required for memory of spatial configuration, but is not required for hippocampus-dependent associative memory.

Discussion

In this study we show that VMAT1 is expressed in mouse brain and plays a key role in survival of hippocampal neurons. Behavioral data demonstrate that mice lacking VMAT1

have neurocognitive deficits. VMAT2 expression is not altered in *VMAT1*KO mice, thus further supporting that VMAT1 plays a unique role in brain function.

Previous studies of VMAT1 brain expression have been conflicting. Hansson et al (1998) found developmental expression of *VMAT1* mRNA in rat brain and Ibanez-Sandoval et al (2010) showed single-cell expression of *VMAT1* mRNA in striatal mouse interneurons. We report in this study *VMAT1* mRNA expression present in WT mouse cortex, striatum, hippocampus and adrenal gland (Fig. 1C). Evidence for VMAT1 protein expression in the adult mammalian brain comes from Lohoff et al (2006) who showed VMAT1-ir in human post-mortem brain and Ashe et al (2011) who showed the presence of VMAT1 protein in various mouse brain regions. In this study, we verified the presence of VMAT1-ir in mouse brain by immunohistochemistry (IHC) with SC15313 (Fig. 2A) and other commercially available antibodies, as well as with a custom designed VMAT1-specific antibody (data not shown). In addition, we carried out colocalization studies using a synaptic marker, that further support VMAT1 brain expression (Figure 2B).

Our findings, and those outlined above, contrast reports suggesting that VMAT1 is only expressed in adult peripheral neuro-endocrine tissue (Peter et al., 1995, Erickson et al., 1996). Differences in experimental methods may explain some of these disparate findings. Immunohistochemistry with numerous antibodies (Figs. 2A, B) and proper antigen retrieval showed VMAT1-ir in cortical, striatal and hippocampal cell bodies of WT, but not *VMAT1*KO mouse brain. No significant VMAT1-ir was observed in *VMAT1*KO mouse adrenal gland as compared to WT littermates (Fig. 2A, panel J-M). Therefore, data from our current methodologies agree with (Ibanez-Sandoval et al., 2010, Ashe et al., 2011), and serve as independent confirmation of *VMAT1* mRNA and protein expression in cell bodies in the adult mouse brain.

Abnormalities in presynaptic neurotransmission might contribute to various neuropsychiatric phenotypes and in fact, research over the last several decades has documented the importance of VMAT2 in neurotransmission and neuropsychiatric disorders (Erickson et al., 1996, Zubieta et al., 2000, Zubieta et al., 2001, Little et al., 2003, Eiden et al., 2004). In contrast to VMAT2 null-mutant mice that die shortly after birth (Fon et al., 1997, Takahashi et al., 1997, Wang et al., 1997, Fumagalli et al., 1999, Narboux-Neme et al., 2011), the VMAT1 KO homozygotes survive into adulthood, suggesting a less severe disruption of monoamine signaling and related brain circuits. We observed enhanced apoptotic cell death in the dentate gyrus of *VMAT1*KO mice (Fig. 3) and no difference in active caspase-3 labeling in the cortex or striatum between WT and *VMAT1KO* mice (Fig. 3B) suggesting a region specific effect of VMAT1 deletion. The observed cell death appears to be by apoptosis as a result of caspase-3 activation (Fig. 3C, 3D). If *VMAT1*KO mice show similar dopamine dysfunction as VMAT2 LO mice, then disruption of VMAT1 handling of dopamine might lead to oxidative stress that could explain the caspase-3 dependent apoptosis in *VMAT1*KO hippocampus; however, whether it is the mitochondrial pathway (*i.e.* caspase-9 dependent) or disruption of other cellular signaling cascades (*i.e.* caspase-8 dependent) that activates the caspase-3 dependent cell death machinery needs further investigation.

VMAT2 is critical to neuronal health by removing neurotransmitter from the cytosol before it can be oxidized (Vergo et al., 2007). We found enhanced apoptosis accompanied by reduced cell proliferation in the hippocampus of *VMAT1*KO mice (Fig. 5) suggesting that VMAT1 may also be important in neurogenesis and the maintenance of neuronal health. Importantly, we observed no differences in *VMAT2* mRNA levels by microarray analysis of striatal mRNA (data not shown) or in other brain regions by RT-PCR (Fig. 7). Furthermore, WT and *VMAT1*KO mice showed no differences in VMAT2 immunostaining in striatum (Fig. 7B, 7C) or in the distribution of VMAT2-specific PET ligand binding in the brain (Fig. 8A, 8B). Consistent with previous literature, VMAT2 in comparison to VMAT1 is higher expressed in all brain regions whereas VMAT1 is higher expressed in adrenal gland (Fig. 7D). Taken together, these data suggest that the enhanced hippocampal apoptosis and reduced cell proliferation are due specifically to *VMAT1* disruption and may point to a brain region-specific effect of VMAT1 absence.

Cognitive deficits are core features of various neuropsychiatric disorders, including affective and psychotic disorders (Harvey et al., 2010, Tamminga et al., 2010). The dentate gyrus generates neurons throughout the lifespan of animals, and this process is critical for the maintenance of neuroplasticity, including responses to stress and learning (Balu et al., 2009). Although most newborn cells in the mouse hippocampus die shortly after generation, ~90% of the surviving cells will develop eventually into neurons that are incorporated into behavioral circuits (Snyder et al., 2009). *VMAT1KO* mice demonstrated reduced proliferation of newborn cells in the hippocampus (Fig. 5) and were deficient in spatial object recognition (Fig. 6), consistent with the notion that disrupted adult neurogenesis *in vivo* contributes to altered memory task performance (Breunig et al., 2007, Reif et al., 2007).

Consolidation of spatial object recognition (SOR) and contextual fear conditioning (CFC) memories has been in both cases linked to hippocampal function in mice (Oliveira et al., 2010) (Frankland et al., 1998). Moreover, adult neurogenesis has been implicated in spatial memory tasks (Madsen et al., 2003, Snyder et al., 2005), and more recently it has been shown to be necessary for pattern discrimination (Sahay et al., 2011). VMAT2-deficient animals have decreased motor function, progressive deficits in olfactory discrimination, shorter latency to behavioral signs of sleep, delayed gastric emptying, anxiety-like behaviors at younger ages, and a progressive depressive-like phenotype (Fukui et al., 2007, Taylor et al., 2011). We observed an effect of VMAT1 deletion on spatial discrimination memory function in the SOR task (Fig. 6A), but no significant effect on the CFC associative memory behavioral task (Fig. 6C); thus, demonstrating a task-specific cognitive decline in adult *VMAT1*KO mice. These data are intriguing and might suggest a link between neuronal loss in the hippocampus and behavioral disturbances observed in *VMAT1*KO mice; however, more experiments are needed to confirm this hypothesis. Consistent with our findings, neurogenesis in the CFC paradigm is implicated not with an associative function, but in contextual discrimination, as ablation of neurogenesis leads to generalization of freezing behavior in an altered context (Sahay et al., 2011, Tronel et al., 2012). Our data indicate that VMAT1 deletion affects a spatial discrimination memory function task, and we speculate that enhanced apoptosis and reduced neurogenesis in VMAT1-deficient mice, due to loss of presynaptic function of VMAT1 in the dentate gyrus, disrupts hippocampal architecture that

could explain the observed behavioral cognitive deficits. Based on the correlated endophenotypes of hippocampal cell loss and cognitive deficits in these mice, the *VMAT1*KO mouse might be useful to further study phenotypes related abnormal neurocognition and memory.

Several limitations to this study should be noted. First, we used mice that were only 8-12 weeks old. Psychiatric disorders are often characterized by strong impairment in the neuronal circuits during brain development, thus the role of VMAT1 at different stages of neuro development needs further investigation. Also, it would be informative to treat *VMAT1*KO mice with various drugs that target monoamine signaling in order to determine if the cognitive deficit in these animals can be improved. Lastly, it is unclear why the *VMAT1* deletion has more pronounced effect in the hippocampus and not in other brain areas. Because VMAT1 has higher expression in the adrenal glands, it remains possible that peripheral stress due to the lack of VMAT1 in the adrenal gland may inhibit neurogenesis and promote apoptosis by activating the hypothalamic-pituitary-adrenal (HPA) axis and thereby preferentially influencing the hippocampus. Future studies are needed to address these questions.

CONFLICT OF INTEREST and ACKNOWLEDGEMENTS

This work was supported by the Center for Neurobiology and Behavior, Department of Psychiatry, University of Pennsylvania. Financial support is gratefully acknowledged from National Institutes of Health grants NIH K08MH080372 (FWL), R01MH86599 (IL) and T32MH14654 (BB). We thank Raymond Meade for assistance with electron microscopy experiments, Seok Rye Choi for help with the biodistribution experiments and Tiffany Smith for technical assistance. Dr. Kung declares that he is named as one of the inventors of a patent involving AV-133. Dr. Lohoff declares that he is named as one of the inventors of a patent (assigned to the University of Pennsylvania) involving human genetic VMAT1 variants (U.S. Pat. No. 7,736,852).

Grant sponsor: NIH; Grant number: K08MH080372 (FWL), R01MH86599 (IL) and T32MH14654 (BB)

References

Ashe KM, Chiu WL, Khalifa AM, Nicolas AN, Brown BL, De Martino RR, Alexander CP, Waggener CT, Fischer-Stenger K, Stewart JK. Vesicular monoamine transporter-1 (VMAT-1) mRNA and immunoreactive proteins in mouse brain. Neuro Endocrinol Lett. 2011; 32:253–258. [PubMed: 21712771]

Balu DT, Hodes GE, Hill TE, Ho N, Rahman Z, Bender CN, Ring RH, Dwyer JM, Rosenzweig-Lipson S, Hughes ZA, Schechter LE, Lucki I. Flow cytometric analysis of BrdU incorporation as a high-throughput method for measuring adult neurogenesis in the mouse. J Pharmacol Toxicol Methods. 2009; 59:100–107. [PubMed: 19121403]

Benes FM, Kwok EW, Vincent SL, Todtenkopf MS. A reduction of nonpyramidal cells in sector CA2 of schizophrenics and manic depressives. Biological psychiatry. 1998; 44:88–97. [PubMed: 9646890]

Bly M. Mutation in the vesicular monoamine gene, SLC18A1, associated with schizophrenia. Schizophrenia research. 2005; 78:337–338. [PubMed: 15961286]

Breunig JJ, Silbereis J, Vaccarino FM, Sestan N, Rakic P. Notch regulates cell fate and dendrite morphology of newborn neurons in the postnatal dentate gyrus. Proceedings of the National Academy of Sciences of the United States of America. 2007; 104:20558–20563. [PubMed: 18077357]

Brunk I, Blex C, Rachakonda S, Holtje M, Winter S, Pahner I, Walther DJ, Ahnert-Hilger G. The First Luminal Domain of Vesicular Monoamine Transporters Mediates G-protein-dependent Regulation of Transmitter Uptake. The Journal of biological chemistry. 2006; 281:33373–33385. [PubMed: 16926160]

Caudle WM, Richardson JR, Wang MZ, Taylor TN, Guillot TS, McCormack AL, Colebrooke RE, Di Monte DA, Emson PC, Miller GW. Reduced vesicular storage of dopamine causes progressive nigrostriatal neurodegeneration. J Neurosci. 2007; 27:8138–8148. [PubMed: 17652604]

Chen SF, Chen CH, Chen JY, Wang YC, Lai IC, Liou YJ, Liao DL. Support for association of the A277C single nucleotide polymorphism in human vesicular monoamine transporter 1 gene with schizophrenia. Schizophrenia research. 2007; 90:363–365. [PubMed: 17223313]

Eiden LE, Schafer MK, Weihe E, Schutz B. The vesicular amine transporter family (SLC18): amine/proton antiporters required for vesicular accumulation and regulated exocytotic secretion of monoamines and acetylcholine. Pflugers Arch. 2004; 447:636–640. [PubMed: 12827358]

Eiden LE, Weihe E. VMAT2: a dynamic regulator of brain monoaminergic neuronal function interacting with drugs of abuse. Ann N Y Acad Sci. 2011; 1216:86–98. [PubMed: 21272013]

Ellis JD, German CL, Birdsall E, Hanson JE, Crosby MA, Rowley SD, Sawada NA, West JN, Hanson GR, Fleckenstein AE. Ephedrine decreases vesicular monoamine transporter-2 function. Synapse. 2011; 65:449–451. [PubMed: 21370280]

Erickson JD, Schafer MK, Bonner TI, Eiden LE, Weihe E. Distinct pharmacological properties and distribution in neurons and endocrine cells of two isoforms of the human vesicular monoamine transporter. Proceedings of the National Academy of Sciences of the United States of America. 1996; 93:5166–5171. [PubMed: 8643547]

Fleckenstein AE, Volz TJ, Hanson GR. Psychostimulant-induced alterations in vesicular monoamine transporter-2 function: neurotoxic and therapeutic implications. Neuropharmacology. 2009; 56(Suppl 1):133–138. [PubMed: 18662707]

Fleckenstein AE, Volz TJ, Riddle EL, Gibb JW, Hanson GR. New insights into the mechanism of action of amphetamines. Annu Rev Pharmacol Toxicol. 2007; 47:681–698. [PubMed: 17209801]

Fon EA, Pothos EN, Sun BC, Killeen N, Sulzer D, Edwards RH. Vesicular transport regulates monoamine storage and release but is not essential for amphetamine action. Neuron. 1997; 19:1271–1283. [PubMed: 9427250]

Frankland PW, Cestari V, Filipkowski RK, McDonald RJ, Silva AJ. The dorsal hippocampus is essential for context discrimination but not for contextual conditioning. Behav Neurosci. 1998; 112:863–874. [PubMed: 9733192]

Fukui M, Rodriguiz RM, Zhou J, Jiang SX, Phillips LE, Caron MG, Wetsel WC. Vmat2 heterozygous mutant mice display a depressive-like phenotype. J Neurosci. 2007; 27:10520–10529. [PubMed: 17898223]

Fumagalli F, Gainetdinov RR, Wang YM, Valenzano KJ, Miller GW, Caron MG. Increased methamphetamine neurotoxicity in heterozygous vesicular monoamine transporter 2 knock-out mice. J Neurosci. 1999; 19:2424–2431. [PubMed: 10087057]

Hall FS, Sora I, Uhl GR. Sex-dependent modulation of ethanol consumption in vesicular monoamine transporter 2 (VMAT2) and dopamine transporter (DAT) knockout mice. Neuropsychopharmacology. 2003; 28:620–628. [PubMed: 12655306]

Hansson SR, Hoffman BJ, Mezey E. Ontogeny of vesicular monoamine transporter mRNAs VMAT1 and VMAT2. I. The developing rat central nervous system. Brain Res Dev Brain Res. 1998; 110:135–158.

Harvey PD, Wingo AP, Burdick KE, Baldessarini RJ. Cognition and disability in bipolar disorder: lessons from schizophrenia research. Bipolar Disord. 2010; 12:364–375. [PubMed: 20636633]

Ibanez-Sandoval O, Tecuapetla F, Unal B, Shah F, Koos T, Tepper JM. Electrophysiological and morphological characteristics and synaptic connectivity of tyrosine hydroxylase-expressing neurons in adult mouse striatum. J Neurosci. 2010; 30:6999–7016. [PubMed: 20484642]

Konradi C, Yang CK, Zimmerman EI, Lohmann KM, Gresch P, Pantazopoulos H, Berretta S, Heckers S. Hippocampal interneurons are abnormal in schizophrenia. Schizophrenia research. 2011; 131:165–173. [PubMed: 21745723]

Little KY, Krolewski DM, Zhang L, Cassin BJ. Loss of striatal vesicular monoamine transporter protein (VMAT2) in human cocaine users. The American journal of psychiatry. 2003; 160:47–55. [PubMed: 12505801]

Liu Y, Peter D, Roghani A, Schuldiner S, Prive GG, Eisenberg D, Brecha N, Edwards RH. A cDNA that suppresses MPP+ toxicity encodes a vesicular amine transporter. Cell. 1992; 70:539–551. [PubMed: 1505023]

Lohoff FW, Dahl JP, Ferraro TN, Arnold SE, Gallinat J, Sander T, Berrettini WH. Variations in the vesicular monoamine transporter 1 gene (VMAT1/SLC18A1) are associated with bipolar i disorder. Neuropsychopharmacology. 2006; 31:2739–2747. [PubMed: 16936705]

Lohoff FW, Lautenschlager M, Mohr J, Ferraro TN, Sander T, Gallinat J. Association between variation in the vesicular monoamine transporter 1 gene on chromosome 8p and anxiety-related personality traits. Neuroscience letters. 2008a; 434:41–45. [PubMed: 18249496]

Lohoff FW, Weller AE, Bloch PJ, Buono RJ, Doyle GA, Ferraro TN, Berrettini WH. Association between polymorphisms in the vesicular monoamine transporter 1 gene (VMAT1/SLC18A1) on chromosome 8p and schizophrenia. Neuropsychobiology. 2008b; 57:55–60. [PubMed: 18451639]

Madsen TM, Kristjansen PE, Bolwig TG, Wortwein G. Arrested neuronal proliferation and impaired hippocampal function following fractionated brain irradiation in the adult rat. Neuroscience. 2003; 119:635–642. [PubMed: 12809684]

McFadden L, Hadlock GC, Allen SC, Vieira-Brock PL, Stout KA, Ellis JD, Hoonakker AJ, Anderyak DM, Neilson SM, Wilkins DG, Hanson GR, Fleckenstein AE. Methamphetamine self-administration causes persistent striatal dopaminergic alterations and mitigates the deficits caused by a subsequent methamphetamine exposure. The Journal of pharmacology and experimental therapeutics. 2011a

McFadden LM, Stout KA, Vieira-Brock PL, Allen SC, Nielsen SM, Wilkins DG, Hanson GR, Fleckenstein AE. Methamphetamine self-administration acutely decreases monoaminergic transporter function. Synapse. 2011b

Narboux-Neme N, Sagne C, Doly S, Diaz SL, Martin CB, Angenard G, Martres MP, Giros B, Hamon M, Lanfumey L, Gaspar P, Mongeau R. Severe serotonin depletion after conditional deletion of the vesicular monoamine transporter 2 gene in serotonin neurons: neural and behavioral consequences. Neuropsychopharmacology. 2011; 36:2538–2550. [PubMed: 21814181]

Need AC, Keefe RS, Ge D, Grossman I, Dickson S, McEvoy JP, Goldstein DB. Pharmacogenetics of antipsychotic response in the CATIE trial: a candidate gene analysis. Eur J Hum Genet. 2009; 17:946–957. [PubMed: 19156168]

Oliveira AM, Hawk JD, Abel T, Havekes R. Post-training reversible inactivation of the hippocampus enhances novel object recognition memory. Learn Mem. 2010; 17:155–160. [PubMed: 20189960]

Peter D, Finn JP, Klisak I, Liu Y, Kojis T, Heinzmann C, Roghani A, Sparkes RS, Edwards RH. Chromosomal localization of the human vesicular amine transporter genes. Genomics. 1993; 18:720–723. [PubMed: 7905859]

Peter D, Liu Y, Sternini C, de Giorgio R, Brecha N, Edwards RH. Differential expression of two vesicular monoamine transporters. J Neurosci. 1995; 15:6179–6188. [PubMed: 7666200]

Reif A, Schmitt A, Fritzen S, Lesch KP. Neurogenesis and schizophrenia: dividing neurons in a divided mind? European archives of psychiatry and clinical neuroscience. 2007; 257:290–299. [PubMed: 17468935]

Richards M, Iijima Y, Kondo H, Shizuno T, Hori H, Arima K, Saitoh O, Kunugi H. Association study of the vesicular monoamine transporter 1 (VMAT1) gene with schizophrenia in a Japanese population. Behav Brain Funct. 2006; 2:39. [PubMed: 17134514]

Sahay A, Wilson DA, Hen R. Pattern separation: a common function for new neurons in hippocampus and olfactory bulb. Neuron. 2011; 70:582–588. [PubMed: 21609817]

Savelieva KV, Caudle WM, Miller GW. Altered ethanol-associated behaviors in vesicular monoamine transporter heterozygote knockout mice. Alcohol. 2006; 40:87–94. [PubMed: 17307644]

Snyder JS, Choe JS, Clifford MA, Jeurling SI, Hurley P, Brown A, Kamhi JF, Cameron HA. Adult-born hippocampal neurons are more numerous, faster maturing, and more involved in behavior in rats than in mice. J Neurosci. 2009; 29:14484–14495. [PubMed: 19923282]

Snyder JS, Hong NS, McDonald RJ, Wojtowicz JM. A role for adult neurogenesis in spatial long-term memory. Neuroscience. 2005; 130:843–852. [PubMed: 15652983]

Soetanto A, Wilson RS, Talbot K, Un A, Schneider JA, Sobiesk M, Kelly J, Leurgans S, Bennett DA, Arnold SE. Association of anxiety and depression with microtubule-associated protein 2- and

synaptopodin-immunolabeled dendrite and spine densities in hippocampal CA3 of older humans. Archives of general psychiatry. 2010; 67:448–457. [PubMed: 20439826]

Stankovski L, Alvarez C, Ouimet T, Vitalis T, El-Hachimi KH, Price D, Deneris E, Gaspar P, Cases O. Developmental cell death is enhanced in the cerebral cortex of mice lacking the brain vesicular monoamine transporter. J Neurosci. 2007; 27:1315–1324. [PubMed: 17287506]

Takahashi N, Miner LL, Sora I, Ujike H, Revay RS, Kostic V, Jackson-Lewis V, Przedborski S, Uhl GR. VMAT2 knockout mice: heterozygotes display reduced amphetamine-conditioned reward, enhanced amphetamine locomotion, and enhanced MPTP toxicity. Proceedings of the National Academy of Sciences of the United States of America. 1997; 94:9938–9943. [PubMed: 9275230]

Tamminga CA, Stan AD, Wagner AD. The hippocampal formation in schizophrenia. The American journal of psychiatry. 2010; 167:1178–1193. [PubMed: 20810471]

Taylor TN, Caudle WM, Miller GW. VMAT2-Deficient Mice Display Nigral and Extranigral Pathology and Motor and Nonmotor Symptoms of Parkinson's Disease. Parkinsons Dis. 2011; 2011:124165. [PubMed: 21403896]

Tong J, Wilson AA, Boileau I, Houle S, Kish SJ. Dopamine modulating drugs influence striatal (+)-[11C]DTBZ binding in rats: VMAT2 binding is sensitive to changes in vesicular dopamine concentration. Synapse. 2008; 62:873–876. [PubMed: 18720517]

Tronel S, Belnoue L, Grosjean N, Revest JM, Piazza PV, Koehl M, Abrous DN. Adult-born neurons are necessary for extended contextual discrimination. Hippocampus. 2012; 22:292–298. [PubMed: 21049483]

Uhl GR, Li S, Takahashi N, Itokawa K, Lin Z, Hazama M, Sora I. The VMAT2 gene in mice and humans: amphetamine responses, locomotion, cardiac arrhythmias, aging, and vulnerability to dopaminergic toxins. FASEB J. 2000; 14:2459–2465. [PubMed: 11099463]

Vergo S, Johansen JL, Leist M, Lotharius J. Vesicular monoamine transporter 2 regulates the sensitivity of rat dopaminergic neurons to disturbed cytosolic dopamine levels. Brain Res. 2007; 1185:18–32. [PubMed: 18028884]

Vieira-Brock PL, Miller EI, Nielsen SM, Fleckenstein AE, Wilkins DG. Simultaneous quantification of nicotine and metabolites in rat brain by liquid chromatography-tandem mass spectrometry. J Chromatogr B Analyt Technol Biomed Life Sci. 2011; 879:3465–3474.

Wang YM, Gainetdinov RR, Fumagalli F, Xu F, Jones SR, Bock CB, Miller GW, Wightman RM, Caron MG. Knockout of the vesicular monoamine transporter 2 gene results in neonatal death and supersensitivity to cocaine and amphetamine. Neuron. 1997; 19:1285–1296. [PubMed: 9427251]

Yamamoto H, Kamegaya E, Hagino Y, Imai K, Fujikawa A, Tamura K, Enokiya T, Yamamoto T, Takeshima T, Koga H, Uhl GR, Ikeda K, Sora I. Genetic deletion of vesicular monoamine transporter-2 (VMAT2) reduces dopamine transporter activity in mesencephalic neurons in primary culture. Neurochem Int. 2007; 51:237–244. [PubMed: 17664021]

Zubieta JK, Huguelet P, Ohl LE, Koeppe RA, Kilbourn MR, Carr JM, Giordani BJ, Frey KA. High vesicular monoamine transporter binding in asymptomatic bipolar I disorder: sex differences and cognitive correlates. The American journal of psychiatry. 2000; 157:1619–1628. [PubMed: 11007716]

Zubieta JK, Taylor SF, Huguelet P, Koeppe RA, Kilbourn MR, Frey KA. Vesicular monoamine transporter concentrations in bipolar disorder type I, schizophrenia, and healthy subjects. Biological psychiatry. 2001; 49:110–116. [PubMed: 11164757]

Interest and significance

- VMAT1 is expressed in mouse brain.
- Deletion of VMAT1 results in reduced neurogenesis and apoptosis in hippocampus.
- VMAT2 expression is not affected by VMAT1 deletion.
- Behavioral experiments show that VMAT1 KO mice have reduced spatial object recognition.

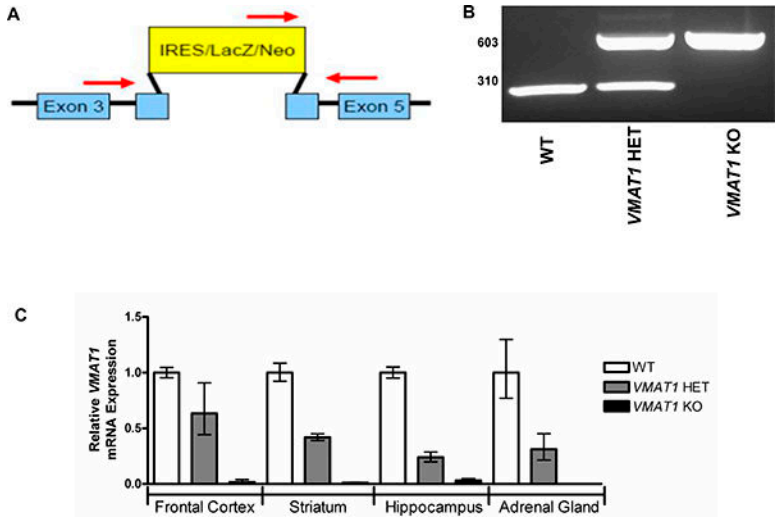

Figure 1. Characterization of *VMAT1* KO mice

(A) Schematic representation of *VMAT1* gene disruption by insertion of an IRES/LacZ/Neo cassette at exon 4 and relative primer (red arrows) positions for genotyping. (B) Genotypes of wild type (WT), heterozygous (*VMAT1* HET) and homozygous knockout (*VMAT1* KO) mice are shown. A 227 base pairs band is expected for WT animals, a 479 base pairs band is expected for *VMAT1* KO animals, and both bands are expected for heterozygotes (*VMAT1* HET). (C) Gene expression analysis for the detection of *VMAT1* mRNA expression in various brain regions and adrenal gland of WT (WT, white bars), heterozygous (*VMAT1* HET, grey bars) and homozygous KO (*VMAT1KO*, black bars) mice. *VMAT1KO* shows complete absence of VMAT1 mRNA expression in the frontal cortex, striatum, hippocampus and adrenal gland with respect to WTs and *VMAT1* HETs. Shown are representative results of two separate quantitative relative mRNA expression experiments, each done in triplicates. Data are expressed as mean ± S.D.

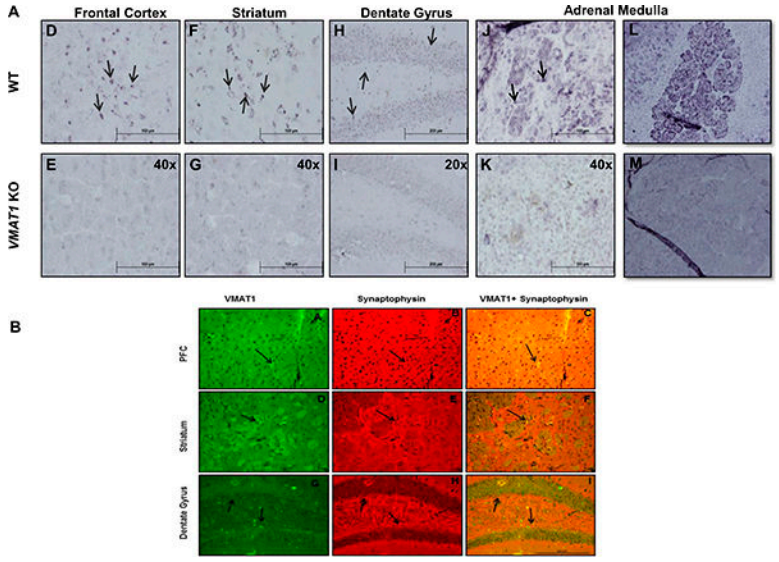

Figure 2. VMAT1 is expressed in various brain regions and adrenal gland

(A) Immunostaining for VMAT1 expression was carried out using antibody SC15313 as detailed in the materials and methods. Digital photomicrographs of VMAT1-immunoreactivity (ir) are shown. Frontal cortex (panels C and D), striatum (panels E and F), dentate gyrus (panels G and H) and adrenal medulla (panels I and J) from WT (WT, panels C, E, G and I) and *VMAT1KO* (*VMAT1KO*, panels D, F, H and J) mice were stained for VMAT1-ir. Ni-DAB staining for VMAT1 localized in neuronal cell bodies (indicated by black arrows) is observed in WT, but not *VMAT1KO* animals. In addition to the SC15313 anti -VMAT1 antibody, VMAT1-ir was confirmed with the use of ab87595 anti-VMAT1 antibody in WT adrenal glands (panel L) and VMAT1 absence in adrenal gland of *VMAT1KO animals* (panel M). Scale bar and magnification for frontal cortex, striatum and adrenal medulla is 100 μm at 40x, and for dentate gyrus is 200 μm at 20x.

(B) Double-immunolabeled fluorescent microscopic 20x magnification images of VMAT1 (green) and synaptophysin (red) in the prefrontal cortex (panel A,B,C), striatum (panel D,E,F) and dentate gyrus (panel G,H,I). Paraffin embedded 6μm brain slices for each of these regions were obtained from WT animals (n=4). VMAT1 (green staining, black arrows) was colabeled with synaptophysin (red staining, black arrows). Representative image of VMAT1 immunoreactive cell body shown in the green with diffuse cytoplasmic staining and a small population of more intense vesicular compartment-like structures shown by synaptophysin labeling (panel B, E and H). Double labeling revealed punctate staining of synaptophysin and VMAT1 with apparent co-localization (Yellow Merge, C, F, I black arrows). Scale bars: A, B, 200 μm.

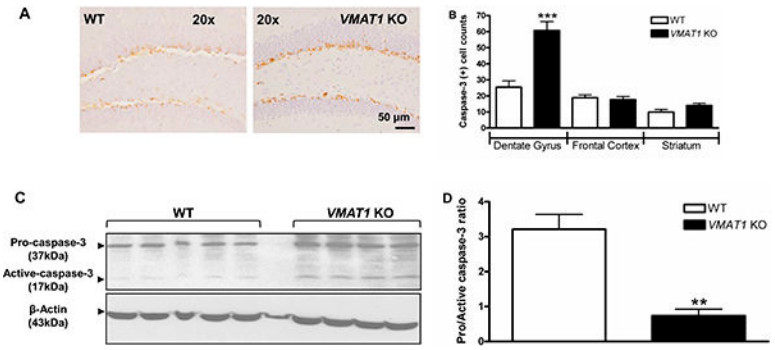

Figure 3. Deletion of *VMAT1* increases neuronal apoptosis

(A) Immunohistochemical detection of caspase-3-positive cells in the hippocampus of WT and *VMAT1KO* mice. Representative images show caspase-3 labeling in the granular cells of the dentate gyrus. 20× magnifications, scale bar is 50 µm. Note the neuronal morphology and caspase-3 labeling in these cells. (B) Quantification of the number of caspase-3 positive cells per 40 µm coronal section in brain regions analyzed (dentate gyrus, cortex and striatum $n = 8$ per group, 4 brain sections per animal). Image-Pro Plus software was used for counting of caspase-3 cells as described in materials and methods. A significant increase in the number of caspase-3 labeled cells was observed in the dentate gyrus of KO (*VMAT1KO*, black bars) as compared to WT (WT, white bars) mice. (C) Western immunoblot detection of pro- (37 kDa) and cleaved, active- caspase-3 (17 kDa) in the cytosolic fractions of hippocampus from WT (WT, left panel) and KO (*VMAT1KO*, right panel) mice brain. The arrowheads indicate both the pro- (37 kDa) and the active- (17 kDa cleaved) caspase-3 fragment, indicative of caspase- 3 activation (upper panels), β-actin (lower panel) served as loading control. (D) Histogram showing quantification of procaspase-3/active caspase-3 ratio in WT (WT, white bars, n=5) and KO (*VMAT1KO*, black bars, n=4) hippocampus. Image J was used to quantify westerns. All histograms were plotted between WT and *VMAT1KO* group Data was analyzed using GraphPad Prism statistical software. Two-tailed non-parametric Student's t-test was employed for the statistical analysis of between-group differences (WT *versus VMAT1KO*). Data are expressed as mean ± S.E.M.; ***p<0.001**p< 0.01.

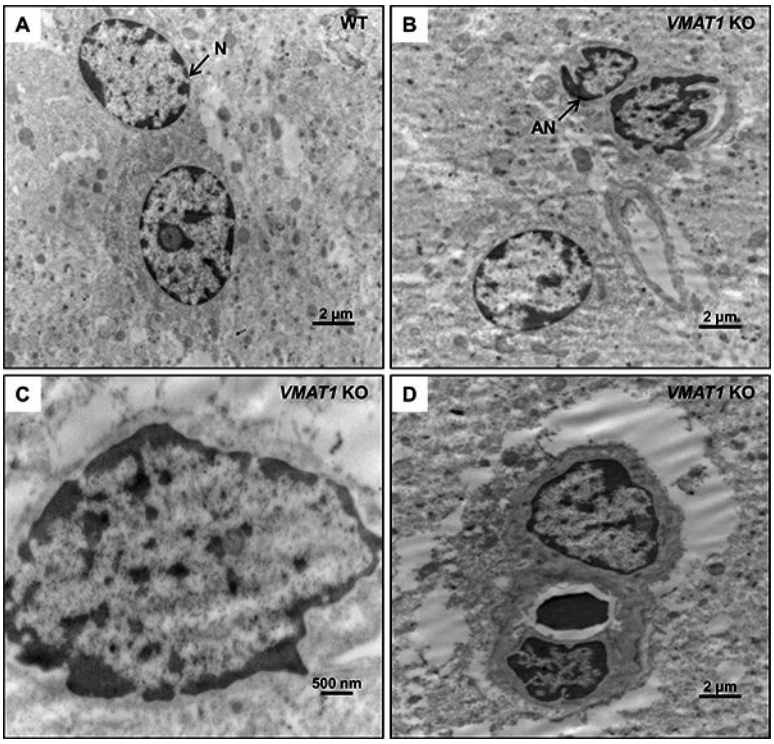

Figure 4. Electron microscopy confirms apoptosis in *VMAT1KO* mice

Electron microscope images show the ultra-structural features of normal nuclei and morphological features of apoptosis in WT (WT, panel A) and KO (*VMAT1KO*, panels B, C and D) dentate gyrus, respectively. Apoptotic cells display (panels B, C and D) plasma membrane blebbing, and partially condensed chromatin in an oval, pyknotic nucleus as morphological features of apoptosis. Original magnifications: (A), (B) and (D) 7500x; Bar=2 µm and (C) 15000x; Bar=500 nm. N=normal nucleus, AN=apoptotic nucleus

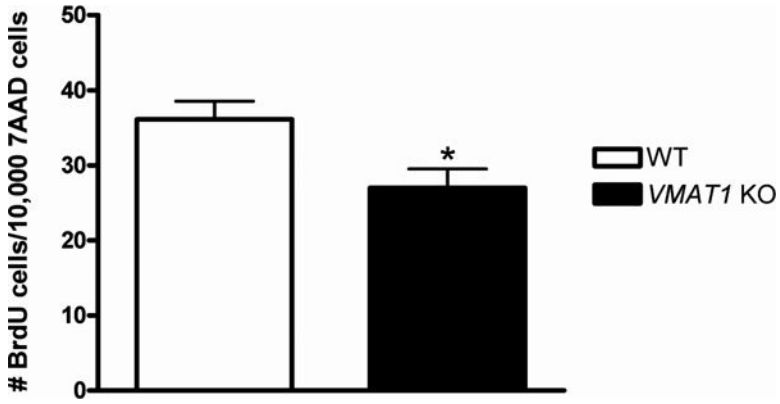

Figure 5. Absence of VMAT1 reduces hippocampal cell proliferation

To assess cell proliferation in the hippocampus, wild type (WT, white bars, n=8) and knockout (*VMAT1* KO, black bars, n=9) mice were sacrificed 24 h after the last BrdU injection. Values are expressed as the number of BrdU positive cells per 10,000 7-AAD events. VMAT1KO mice demonstrated a significant reduction of BrdU incorporation in the hippocampus compared to WT mice ($t(16) = 2.78$, $p=0.01$). Data was analyzed using GraphPad Prism statistical software. Two-tailed non-parametric Student's t-test was employed for the statistical analysis of between-group differences (wild type versus *VMAT1* KO). Data are shown as mean ± S.E.M.; *p=0.01.

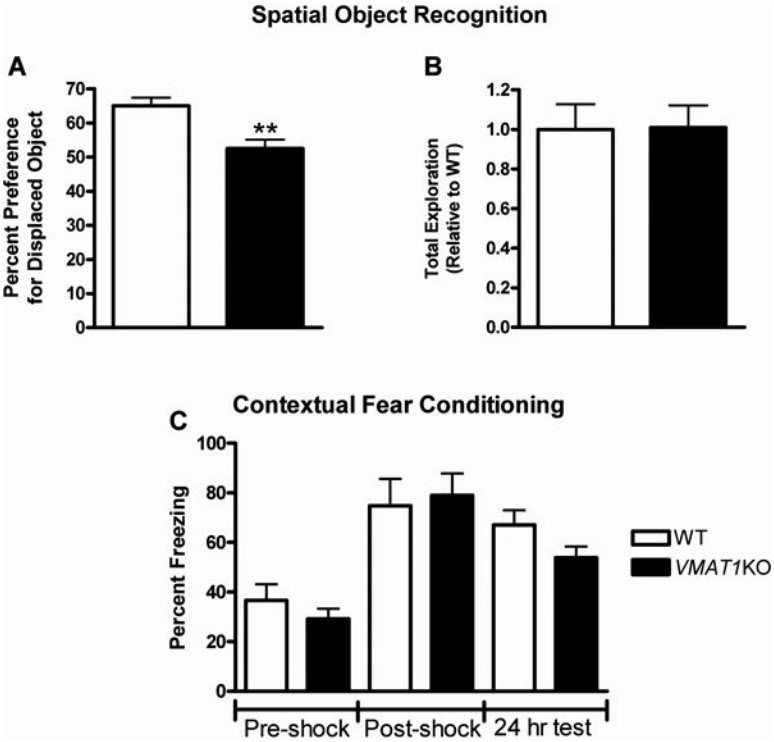

Figure 6. *VMAT1KO* mice show deficits in spatial object recognition, but not in contextual fear conditioning memory

(A) Percentage of the preference for the displaced object by WT (WT, white bars, *n*=12) and KO (*VMAT1KO*, black bars, *n*=12) mice. (B) Total exploration of objects by WT (WT, white bars, *n*=12) and KO (*VMAT1KO*, black bars, *n*=12) mice. (C) Freezing percentage of WT (WT, white bars, *n*=8) and KO (*VMAT1KO*, black bars, *n*=8) mice on contextual fear conditioning test. Pre- and post-shock data represent baseline and immediate, unconditioned responses before and after foot shock, respectively. Freezing behavior in the conditioned context test session 24h after training is also shown. Data was analyzed using GraphPad Prism statistical software. Two-tailed non-parametric Student's t-test was employed for the statistical analysis of between-group differences (WT versus *VMAT1KO*). Data are expressed as mean ± S.E.M.; ***p*<0.01.

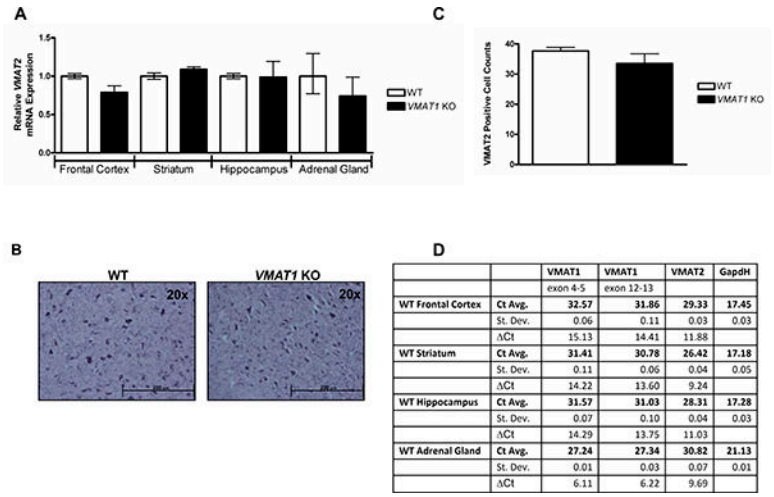

D

		VMAT1	VMAT1	VMAT2	GapdH
		exon 4-5	exon 12-13		
WT Frontal Cortex	**Ct Avg.**	**32.57**	**31.86**	**29.33**	**17.45**
	St. Dev.	0.06	0.11	0.03	0.03
	ΔCt	15.13	14.41	11.88	
WT Striatum	**Ct Avg.**	**31.41**	**30.78**	**26.42**	**17.18**
	St. Dev.	0.11	0.06	0.04	0.05
	ΔCt	14.22	13.60	9.24	
WT Hippocampus	**Ct Avg.**	**31.57**	**31.03**	**28.31**	**17.28**
	St. Dev.	0.07	0.10	0.04	0.03
	ΔCt	14.29	13.75	11.03	
WT Adrenal Gland	**Ct Avg.**	**27.24**	**27.34**	**30.82**	**21.13**
	St. Dev.	0.01	0.03	0.07	0.01
	ΔCt	6.11	6.22	9.69	

Figure 7. Deletion of *VMAT1* does not affect VMAT2 expression

(A) Gene expression analysis for the detection of *VMAT2* in various brain regions and adrenal gland of wild type (WT, white bars) and homozygous *VMAT1* KO (*VMAT1* KO, black bars) mice. No difference in *VMAT2* mRNA expression was observed between the WT and *VMAT1* KO mouse brain regions or adrenal glands. Shown are the representative results of two separate quantitative relative mRNA expression experiments, each done in triplicates. (B) Ni-DAB immunostaining for VMAT2 expression in coronal sections of the striatum was done using VMAT2 specific antibody as described in the materials and methods. Digital photomicrographs of VMAT2-immunoreactivity from wild type (WT) and *VMAT1* knockout (*VMAT1* KO) mice striatum are shown. Scale bar and magnification for striatum is 200 μm at 20×. (C) Quantification of VMAT2-immunolabelled cell counts in the striatum (four brain sections per animal). No statistical difference between the wild type (WT, white bars, n=5) and *VMAT1* knockout (*VMAT1* KO, black bars, n=5) was observed for the VMAT2-positive cell counts in the striatum. Image-Pro Plus software was used for the counting of VMAT2 labeled cells as described in materials and methods. Two-tailed non-parametric Student's t-test was employed for the statistical analysis between-group differences (wild type versus *VMAT1* KO). Data are expressed as means ± S.E.M. (D) Gene expression analysis for the detection of *VMAT1* and *VMAT2* mRNA expression in various brain regions and adrenal gland of WT mice. VMAT2 is highest expressed in striatum whereas VMAT1 shows strong expression in adrenal gland. Shown are results of qPCR mRNA expression analyses, each done in triplicates. Average Ct and delta Ct values are shown.

A

[18F]AV-133	WT		VMAT1KO		VMAT2KO	
%dose/g	AVG	SD	AVG	SD	AVG	SD
BLOOD	**1.11**	0.09	**1.09**	0.11	**1.11**	0.08
KIDNEY	**3.96**	0.39	**3.56**	0.14	**3.00**	1.06
LIVER	**15.97**	2.75	**14.28**	1.34	**15.45**	0.94
PANCREAS	**9.46**	1.25	**8.80**	0.58	**7.60**	3.11
BONE	**9.35**	2.10	**8.22**	0.69	**4.89**	0.76
BRAIN	**0.98**	0.08	**0.84**	0.11	**0.61**	0.03
%iD/g	AVG	SD	AVG	SD	AVG	SD
Cerebellum	**0.583**	0.082	**0.467**	0.113	**0.386***	0.036
Hippocampus	**0.847**	0.040	**0.714**	0.183	**0.459***	0.056
Striatum	**1.602**	0.167	**1.540**	0.172	**0.940***	0.127
Cortex	**0.650**	0.073	**0.442**	0.111	**0.453***	0.037
Remainder	**0.996**	0.120	**0.866**	0.075	**0.671***	0.045
Ratio	AVG	SD	AVG	SD	AVG	SD
Cerebellum	**1.00**	0.00	**1.00**	0.00	**1.00**	0.00
Hippocampus	**1.47**	0.19	**1.53**	0.10	**1.21**	0.25
Striatum	**2.83**	0.73	**3.42**	0.82	**2.43**	0.12
Cortex	**1.14**	0.27	**0.95**	0.13	**1.18**	0.15
Remainder	**1.72**	0.20	**1.92**	0.39	**1.75**	0.16

B

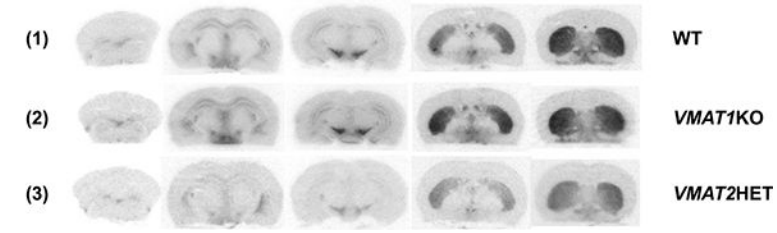

Figure 8. *Ex vivo* autoradiography with [^{18}F]AV-133 shows no difference in the VMAT2 labeling

(A) Quantitative distribution of PET ligand in various brain regions. The distribution of [^{18}F]-AV-133 was measured in wild type (WT), *VMAT1* KO and *VMAT2* heterozygote (24-33g, 8-12 weeks old, n=4 per group). The percentage dose per gram of tissue was calculated by a comparison of the tissue counts to diluted aliquots of the injected material. T-tests were done only for regional brain distribution data. *p<0.05 (B) Localization of PET ligand in various brain regions of (1) wild type (WT) (2) *VMAT1* KO (3) *VMAT2* Het (n=4 per group). Sections were exposed to Biomax MR films overnight and processed with Kodak fixer and developer. Images were digitized with an Epson Perfection 4490 Photo scanner.